

A longer *XMM-Newton* look at I Zwicky 1: Variability of the X-ray continuum, absorption, and iron $K\alpha$ line

L. C. Gallo,¹ W. N. Brandt,² E. Costantini,^{3,4} A. C. Fabian,⁵ K. Iwasawa,¹
and I. E. Papadakis⁶

¹ *Max-Planck-Institut für extraterrestrische Physik, Postfach 1312, 85741 Garching, Germany*

² *Department of Astronomy and Astrophysics, The Pennsylvania State University, 525 Davey Lab, University Park, PA 16802, USA*

³ *SRON National Institute for Space Research Sorbonnelaan 2, 3584 CA Utrecht, The Netherlands*

⁴ *Astronomical Institute, Utrecht University, P.O. Box 80000, 3508 TA Utrecht, The Netherlands*

⁵ *Institute of Astronomy, University of Cambridge, Madingley Road, Cambridge CB3 0HA*

⁶ *Physics Department, University of Crete, P.O. Box 2208, 710 03 Heraklion, Crete, Greece*

Accepted. Received.

ABSTRACT

We present the second *XMM-Newton* observation (85 ks) of the narrow-line Seyfert 1 galaxy (NLS1) I Zw 1 and describe its mean spectral and timing characteristics. On average, I Zw 1 is ~ 35 per cent dimmer in 2005 than in the shorter (20 ks) 2002 observation. Between the two epochs the intrinsic absorption column density diminished, but there were also subtle changes in the continuum shape. Considering the blurred ionised reflection model, the long-term changes can be associated with a varying contribution of the power law component relative to the total spectrum. Examination of normalised light curves indicates that the high-energy variations are quite structured and that there are delays, but only in some parts of the light curve. Interestingly, a hard X-ray lag first appears during the most-distinct structure in the mean light curve, a flux dip ~ 25 ks into the observation. The previously discovered broad, ionised Fe $K\alpha$ line shows significant variations over the course of the 2005 observation. The amplitude of the variations is 25 – 45 per cent and they are unlikely due to changes in the Fe $K\alpha$ -producing region, but perhaps arise from orbital motion around the black hole or obscuration in the broad iron line-emitting region. The 2002 data are re-examined for variability of the Fe $K\alpha$ line at that epoch. There is evidence of energy and flux variations that are associated with a hard X-ray flare that occurred during that observation.

Key words: galaxies: active – galaxies: nuclei – quasars: individual: I Zw 1 – X-ray: galaxies

1 INTRODUCTION

I Zw 1 ($z = 0.0611$) is considered the prototypical narrow-line Seyfert 1 galaxy (NLS1) mainly due to its distinct optical properties. At X-ray energies the active galactic nucleus (AGN) exhibits behaviour that is somewhat more modest than for typical NLS1s (e.g. Leighly 1999a, 1999b). However, a short (20 ks) *XMM-Newton* observation conducted in 2002 revealed a plethora of interesting characteristics, such as: hard X-ray flaring, unresolved transition array (UTA) absorption, and possibly multiple Fe $K\alpha$ emission lines (Gallo et al. 2004a, hereafter G04).

The discoveries in G04 prompted further examination with a second longer *XMM-Newton* observation. This is the first of three papers which describe the X-ray properties of I Zw 1 utilising all *XMM-Newton* data. In this work, we present an 85 ks *XMM-Newton* observation and describe the mean spectral and timing characteristics of the AGN, as well as compare the data to the earlier 2002 observation. The complex ionised absorber and its long-term vari-

ability is discussed in detail in the work of Costantini et al. (2007). In addition, I Zw 1 exhibits remarkable short-term spectral variability during the 2005 observation. This is presented in Gallo et al. (2007).

2 OBSERVATIONS AND DATA REDUCTION

I Zw 1 was observed for the second time by *XMM-Newton* (Jansen et al. 2001) on 2005 July 18–19 during revolution 1027 (obsid 0300470101) (hereafter we will refer to this as the 2005 observation). The total duration was 85 ks, during which time all instruments were functioning normally. The EPIC pn (Strüder et al. 2001) and MOS (MOS1 and MOS2; Turner et al. 2001) cameras were operated in small-window mode with the medium filter in place. The Reflection Grating Spectrometers (RGS1 and RGS2; den Herder et al. 2001) also collected data during this time, as did the Optical Monitor (OM; Mason et al. 2001).

The Observation Data Files (ODFs) from the 2002 and 2005 observations were processed to produce calibrated event lists using the *XMM-Newton* Science Analysis System (SAS v7.0.0). Unwanted hot, dead, or flickering pixels were removed as were events due to electronic noise. Event energies were corrected for charge-transfer inefficiencies. EPIC response matrices were generated using the SAS tasks ARFGEN and RMFGEN. Light curves were extracted from these event lists to search for periods of high background flaring. Some background flaring detected toward the end of the 2005 observation, and the data during those periods have been neglected. The total amount of good exposure time selected was 58 ks and 82 ks for the pn and MOS detectors, respectively. Source photons were extracted from a circular region $35''$ across and centred on the source. The background photons were extracted from an off-source region and appropriately scaled to the source-selection region. Single and double events were selected for the pn detector, and single-quadruple events were selected for the MOS. The total number of source counts collected by the pn instrument in the 0.3 – 10 keV range was approximately 2.75×10^5 . In the 0.5 – 10 keV band, the MOS instruments collected about 8.4×10^4 (MOS1) and 8.9×10^4 (MOS2) source counts. Comparing the source and background spectra we found that the spectra are source dominated below 10 keV.

The RGS were operated in standard Spectro+Q mode in 2005, and a total exposure of 85 ks was collected. The first-order RGS spectra were extracted using the SAS task RGSPROC, and the response matrices were generated using RGSRMFGEN. The estimated number of source counts collected in the 0.35 – 2 keV range were approximately 10220 and 11920 for the RGS1 and RGS2, respectively. The RGS data are used in the analysis of the ionised absorber in I Zw 1 (Costantini et al. 2007) and will not be discussed here.

During 2005, I Zw 1 was observed with the OM in Fast-mode through four filters (*U*, *UVW1*, *UVW2* and *UVM2*). The purpose was to examine possible optical variability. Unfortunately, the AGN was not well centred in the small, fast-mode, frame and fell close to the detector edge. Consequently, optical variability could not be examined in a robust manner.

3 2005 X-RAY LIGHT CURVES

During the 20 ks 2002 observation I Zw 1 exhibited a modest X-ray flare, which lasted a total of ~ 5 ks (G04). Notably the flare appeared to be quite hard, concentrated in the 3 – 12 keV band, thus inducing spectral variability. Aside from this lone event the light curve was relatively quiet in comparison to many NLS1.

The 2005 light curve appears more active, consistently variable with, on average, larger amplitudes than observed in 2002 (Figure 1). Perhaps the most interesting event in the light curve is the sharp drop about 25 ks into the observation. There is spectral variability related to the light curve, and this is discussed at length in Gallo et al. (2007). Here, we will focus on the flux variations.

Light curves were created in three energy bands: 0.2 – 0.7 keV, 2 – 3 keV and 3 – 12 keV. As will be demonstrated in the spectral analysis, the softest band is the region where both the power law component and the soft excess component influence the spectrum. Both higher bands are dominated by the power law component alone.

Using the light curves in 1000 s bins, each of the high-energy light curves was cross-correlated (following Edelson & Krolik 1988) with the the 0.2 – 0.7 keV band to search for possible lags (positive delay means hard-band lags the soft-band). All of the

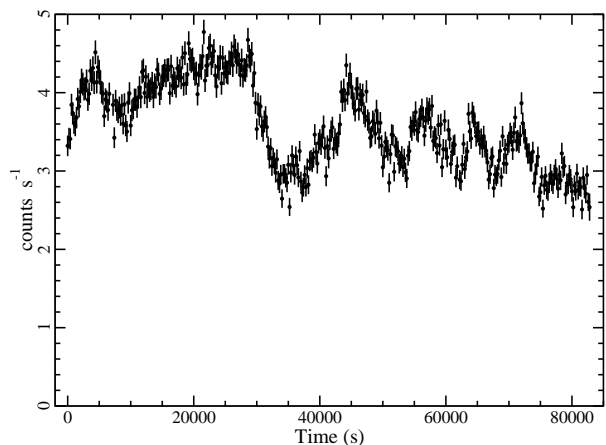


Figure 1. The 2005 0.2 – 12 keV EPIC pn light curve in 200 s bins. The start time corresponds to the beginning of the pn exposure.

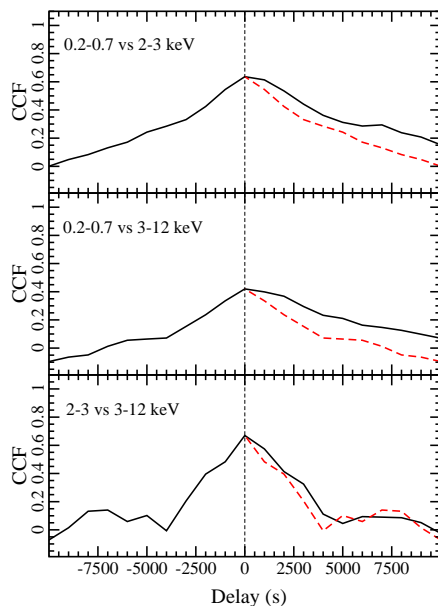


Figure 2. The CCF from cross-correlating the energy bands shown in each panel. In each panel the negative delay curve is reflected about the zero axis and shown as a red, dashed curve on the positive side. This is done to highlight the asymmetry of the CCFs toward positive lags meaning that the soft bands are leading the variations.

cross-correlation functions (CCFs) were asymmetric toward positive lags (Figure 2).

There are a few AGN where time delays as a function of Fourier frequency (see Nowak et al. 1999 and references therein for details) have been determined (see Papadakis et al. 2001 for the first reported detection in an AGN). If there were a *single* delay between the light curves in the various energy bands, then the time delay between all of the Fourier frequencies would be the same. In contrast, what is typically observed is that as the frequency of the Fourier components decreases, the delays increase. Furthermore, as

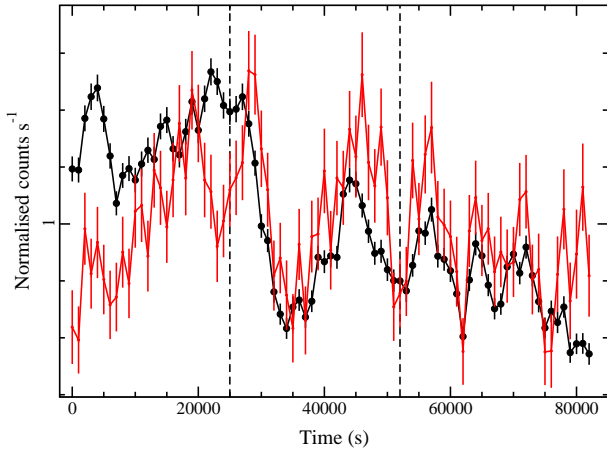


Figure 3. Light curves in the 0.2 – 0.7 keV (black dots) and 3 – 12 keV bands normalised to their respective means. A hard band lag is apparent in between $\sim 25 - 52$ ks. The start time corresponds to the beginning of the pn exposure.

the energy band separation between two light curves increases, the delays, at the same frequency, also increase (e.g. see Arévalo et al. 2006 for a recent discussion).

In the case of I Zw 1, we cannot estimate time lags as a function of frequency due to limit signal in the hard-band light curve. However, the CCFs are consistent with what we observe in other AGN and NLS1. The CCFs show broad humps around zero time lag with an asymmetry toward positive lags, but not a single, distinct delay. This is consistent with the hypothesis that in I Zw 1, just like in other Seyferts, the sine and cosine functions in the hard-band light curves are delayed with respect to those in the soft-band light curves, but the delay is not the same for all of them: the delays increase with decreasing frequency and increased separation between the energy bands.

Of interest may be the particularly small values measured in the CCFs (0.5 – 0.7). We examine this further by directly comparing light curves in each energy band normalised to their respective mean (Figure 3). Most obvious in the comparison between the 0.2 – 0.7 keV and 3 – 12 keV band is the significance of the delay between $\sim 25 - 55$ ks. In particular, the delay seemingly begins at the onset of the sharp dip in the light curve. If we calculate the CCF in this time regime alone we see a clear dominant lag at ~ 1 ks (Figure 4).

However, as Figure 3 demonstrates, the lag is not always present. Sometimes there are no delays, and at other times the light curves show different behaviour and even anti-correlations (e.g. $\sim 20 - 25$ ks and > 75 ks into the observation). All of these factors contribute to the small value of the CCF peaks. Similar behaviour was seen in the NLS1 IRAS 13224–3809 (Gallo et al. 2004b) where the authors suggested possible alternating lags between high- and low-energy bands (i.e. sometimes hard band lags and other times it leads).

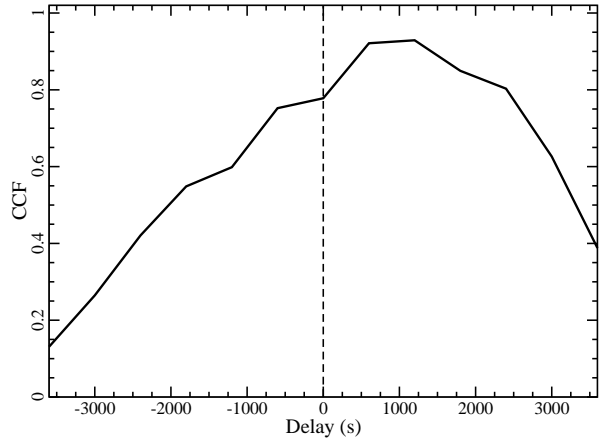


Figure 4. The CCF when cross-correlating the 0.2 – 0.7 keV and 3 – 12 keV light curves between 25 – 55 ks only. A hard band lag appears more dominant in this time band and peaks at ~ 1 ks.

4 A COMPARISON OF THE 2002 AND 2005 SPECTRA

4.1 Summary of the 2002 observation

The 0.2 – 10 keV spectrum of I Zw 1 has long been known to differ from those of other NLS1. It possesses a rather weak soft excess and is modified by intrinsic neutral and ionised absorption. The 2002 observation of I Zw 1 (G04) was rather typical of what had been seen previously (e.g. Leighly 1999a, b).

There were several simple continuum models (e.g. blackbody plus power law, broken power laws) that when modified by intrinsic ionised absorption (an absorption-edge), neutral absorption (absorption column density) and an Fe $K\alpha$ emission line, fit the EPIC spectra adequately in 2002. None of these continuum models stood out as superior. Since the 2002 data were reprocessed with the newest calibration we refit the simple models to the newly processed data and find comparable results. The one modification was in the intrinsic absorption column density, which was slightly lower with the new calibration ($N_{\text{H}} = 5 \times 10^{20} \text{ cm}^{-2}$ as opposed to $N_{\text{H}} = 10 \times 10^{20} \text{ cm}^{-2}$).

A particularly interesting spectral result from the 2002 observation was the possible presence of multiple iron lines. In addition to a broad and ionised line, the spectrum also required a narrow, unresolved emission line at 6.4 keV. The most obvious interpretation adopted by G04 was that this feature was produced in distant material such as the torus.

4.2 Spectral changes since 2002

The 2005 spectrum does appear substantially different from the 2002 observation. The broad-band differences between 2002 and 2005 can be depicted by extrapolating the best-fit 2–10 keV power law to both spectra down to lower energies (Figure 5).

The 2005 observation shows a much softer spectrum, a suggestion that the level of absorption may have changed since 2002. The best-fitting power law in the 2 – 10 keV band is slightly flatter in 2005 ($\Gamma = 2.15 \pm 0.02$ compared to $\Gamma = 2.28 \pm 0.03$ in 2002), which likely also contributes to the apparently stronger soft excess at that epoch. The inset in Figure 5 shows the residuals in the Fe $K\alpha$ band. As with previous observations, the iron line appears

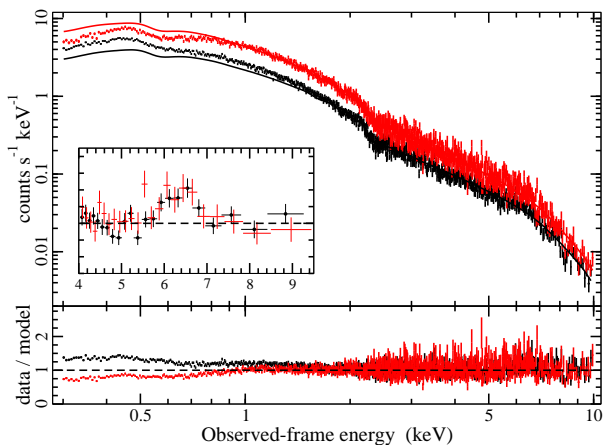


Figure 5. Top panel: Best-fit power law modelled to the 2002 (red marks, $\Gamma = 2.28 \pm 0.03$) and 2005 (black marks, $\Gamma = 2.15 \pm 0.02$) 2 – 10 keV spectrum, and extrapolated to 0.3 keV. Lower panel: Resulting ratio from the above model. Top panel (inset): Ratio in the 4 – 9.5 keV band, binned for display purposes. The scale on the y-axis is from 0.7 – 1.45.

broad and ionised. The agreement in the appearance of the iron line at both epochs is good.

We applied the blackbody plus power law model from 2002 to the 2005 data to examine consistency between the two epochs. Simply rescaling the model was unacceptable ($\chi^2_{\nu}/\text{dof} = 5.7/846$). Allowing the level of neutral absorption to vary freely significantly improves the fit quality ($\chi^2_{\nu}/\text{dof} = 1.27/845$) indicating that the column density of the neutral absorber has dropped in 2005 to $N_{\text{H}} \approx 1.4 \times 10^{20} \text{ cm}^{-2}$. Allowing the low-energy absorption edge to vary in energy and depth is a further improvement ($\Delta\chi^2 = 36.2$ for 2 additional free parameters). The overall fit is not acceptable ($\chi^2_{\nu}/\text{dof} = 1.23/843$) and demonstrates that subtle changes in the intrinsic continuum shape since 2002 may be appropriate.

If rather we consider a constant absorber and allow only the continuum parameters to vary, we obtain a worse fit ($\chi^2_{\nu}/\text{dof} = 1.35/843$). Indeed variable absorbers seem necessary and are supported by the RGS data. The absorption in I Zw 1 is treated in detail by Costantini et al. (2007).

5 2005 SPECTRAL MODELLING

The source spectra were grouped such that each bin contained at least 20 counts (typically more). Spectral fitting was performed using XSPEC v11.3.0 (Arnaud 1996). All parameters are reported in the rest frame of the source unless specified otherwise. The quoted errors on the model parameters correspond to a 90% confidence level for one interesting parameter (i.e. a $\Delta\chi^2 = 2.7$ criterion). A value for the Galactic column density toward I Zw 1 of $5.07 \times 10^{20} \text{ cm}^{-2}$ (Elvis et al. 1989) is adopted in all of the spectral fits. K-corrected luminosities are calculated using a Hubble constant of $H_0 = 70 \text{ km s}^{-1} \text{ Mpc}^{-1}$ and a standard flat cosmology with $\Omega_M = 0.3$ and $\Omega_{\Lambda} = 0.7$.

In the analysis of the 2002 data, G04 were able to fit the spectra with various phenomenological models, but could not distinguish a superior one. While they were able to establish that a second, soft component was a necessary part of the continuum they

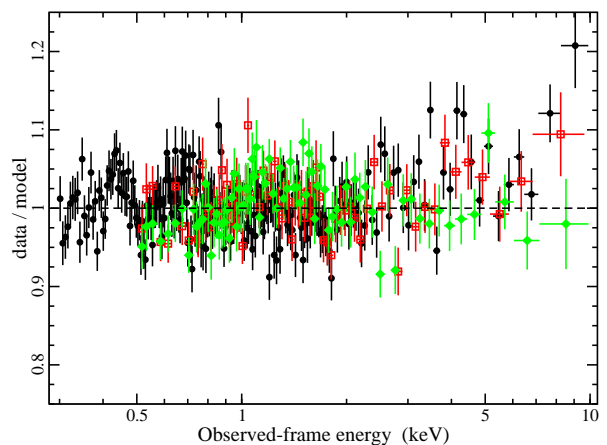


Figure 6. The residuals (data/model) from fitting a model composed of a blackbody, power law and Gaussian profile (modified by absorption) to the EPIC data (see third row in Table 1). Black dots, red open squares, and green diamonds correspond to the pn, MOS1, and MOS2 data, respectively. The data are rebinned for display purposes.

were unable to determine whether the soft excess was curved (e.g. blackbody-like) or flat (power law-like).

5.1 The 2-10 keV spectra

As was done for the 2002 data (G04), we built-up a broad-band spectral model for the 2005 observation utilising all the EPIC data. Fitting the 2 – 10 keV EPIC spectra with a single power law (each instrument having free photon index (Γ) and normalisation to accommodate existing cross-calibration uncertainties) resulted in a satisfactory model ($\chi^2_{\nu}/\text{dof} = 1.03/1090$). Adding a Gaussian profile to this continuum, with a common energy (E) and width (σ) among all three instruments was a significant improvement ($\Delta\chi^2 = 59.5$ for 5 free additional parameters). The best fit line parameters were $E = 6.70 \pm 0.14 \text{ keV}$, $\sigma = 523^{+276}_{-157} \text{ eV}$ and $EW_{\text{pn}} = 265^{+105}_{-32}$, $EW_{\text{M1}} = 220^{+130}_{-49}$, $EW_{\text{M2}} = 239^{+191}_{-79} \text{ eV}$. G04 introduced the possibility of multiple line features in the Fe K α region of the 2002 spectrum, including an intrinsically narrow 6.4 keV line. No such line is present in the 2005 spectrum. A narrow, neutral line is completely insignificant in the pn spectrum and any such feature in the MOS has an $EW < 27 \text{ eV}$.

A comparable improvement ($\Delta\chi^2 = 38.0$ for 5 free additional parameters) can be achieved if a disc line profile (Fabian et al. 1989) rather than a Gaussian profile is used for the broad residuals. In this case the best-fit energy and inner disc radius are $E = 6.55^{+0.20}_{-0.10} \text{ keV}$ and $R_{\text{in}} = 6 - 26$ gravitational radii, respectively. The disc inclination (i) is fixed at 50° , to remain consistent with our finding in Section 6.1. Leaving the parameter free to vary does not enhance the fit statistics, nor does it affect the best-fit line energy. The line strength is $EW \approx 200 \text{ eV}$ in each spectrum. For simplicity, we adopt the Gaussian profile.

5.2 Simple broad-band models

Extrapolating the 2 – 10 keV fit to 0.3 keV in the pn and 0.5 keV in the two MOS left a gradual rise in the residuals that is typically associated with the soft excess.

Table 1. Fit parameters for the simple models (column 1) applied to the 2005 full-band data. Fit quality is given in column 2. Neutral absorption intrinsic to I Zw 1 is given in column 3 ($\times 10^{20} \text{ cm}^{-2}$). In column 4, the continuum parameters are shown. If the parameter is not linked between the various instruments it is identified as pn, M1 (MOS1) and M2 (MOS2). E_b is the break energy (in keV) for the broken power law model. The photon index above (Γ_h) and below (Γ_s) the break energy are also shown. The blackbody temperature (kT) is given in eV. Column 5 provides the absorption-edge parameters: energy (E) and optical depth (τ). All fits except for the partial covering model (second row) include an FeK α emission line with comparable parameters to the results presented in the text. The line was not statistically necessary in the partial covering model. The parameters of the partial covering absorber, column density ($N_{\text{Hpc}}, \times 10^{22} \text{ cm}^{-2}$) and covering fraction (f), are given in column 6.

(1) Model	(2) χ^2_ν/dof	(3) $N_{\text{H}i}$	(4) Continuum	(5) Edge	(6) Partial absorber
Single power law	1.13/1628	$0.71^{+0.23}_{-0.20}$	$\Gamma_{pn} = 2.37 \pm 0.01$ $\Gamma_{M1} = 2.29^{+0.02}_{-0.01}$ $\Gamma_{M2} = 2.30^{+0.02}_{-0.01}$	$E = 644^{+9}_{-10}$ $\tau = 0.15 \pm 0.02$	
Single power law with partial covering	1.08/1629	$1.62^{+0.28}_{-0.31}$	$\Gamma_{pn} = 2.43 \pm 0.06$ $\Gamma_{M1} = 2.35 \pm 0.01$ $\Gamma_{M2} = 2.37 \pm 0.01$	$E = 648^{+6}_{-9}$ $\tau = 0.19 \pm 0.02$	$N_{\text{Hpc}} = 31.5^{+7.6}_{-4.1}$ $f = 0.72^{+0.09}_{-0.06}$
Broken power law	1.08/1626	$2.13^{+0.31}_{-0.38}$	$\Gamma_s = 2.48 \pm 0.03$ $E_b = 1.89^{+0.23}_{-0.10}$ $\Gamma_{h,pn} = 2.27^{+0.02}_{-0.03}$ $\Gamma_{h,M1} = 2.17^{+0.03}_{-0.05}$ $\Gamma_{h,M2} = 2.35 \pm 0.03$	$E = 648^{+6}_{-9}$ $\tau = 0.20 \pm 0.02$	
Blackbody plus power law	1.08/1626	< 0.20	$kT = 216 \pm 12$ $\Gamma_{pn} = 2.30 \pm 0.01$ $\Gamma_{M1} = 2.21 \pm 0.01$ $\Gamma_{M2} = 2.23 \pm 0.01$	$E = 651^{+7}_{-9}$ $\tau = 0.20 \pm 0.02$	
Double power law	1.04/1626	$3.22^{+0.69}_{-0.27}$	$\Gamma_1 = 2.67^{+0.05}_{-0.04}$ $\Gamma_{2,pn} = 1.43^{+0.16}_{-0.06}$ $\Gamma_{2,M1} = 1.74^{+0.12}_{-0.04}$ $\Gamma_{2,M2} = 2.03^{+0.13}_{-0.06}$	$E = 652^{+6}_{-10}$ $\tau = 0.18 \pm 0.02$	

The entire 2005 0.3–10 keV band was modelled with various continuum models. Through repeated effort we found it necessary to include in all models an additional neutral absorber at the redshift of the source, as well as a low-energy (~ 650 eV) absorption edge that mimics the more complicated ionised absorption. As with the 2002 fits, the phenomenological models demonstrate the necessity of an additional soft component, but we cannot distinguish various models (see Table 1).

As with the 2002 observation, the 2005 data show that a second continuum component is required to fit the spectrum of I Zw 1. According to an F -test, the addition of a second continuum component (i.e. 2 additional parameters) to a single power law is highly significant (F -test probability $\sim 10^{-17}$). Also like the 2002 observation, a single superior model does not stand out. However, there are similarities among all the models in Table 1. One may notice that the second component is not highly curved. Even in the case of the blackbody plus power law model, the high-temperature of the blackbody component will give it a flatter appearance in the EPIC bandpass.

Of interest is that there is detectable diminishing of the intrinsic column density in I Zw 1 since 2002. The exact change depends on what continuum model is assumed, but appears to be at least on the 50 per cent level.

The residuals from the blackbody plus power law fit are shown in Figure 6. Notable in Figure 6 are the positive residuals, which remain in the fit above ~ 8 keV. These residuals are apparent in all broad-band fits to the 2005 data (see also Figure 7 and the lower

panel of Figure 8), with the exception of the double power law model. The most likely cause is the significant spectral variability exhibited by I Zw 1 in 2005 (Gallo et al. 2007). Gallo et al. suggest that the power law photon index could be changing during the 2005 observation, which would explain the difficulty in fitting the average spectrum with a single power law. The reason that the residuals are minimal in the double power law model could simply be that the second power law does not begin to dominate the spectrum until rather high energies (~ 5.5 keV in the pn spectrum).

Based on the blackbody plus power law model, the average 0.3–10 keV flux during 2005, corrected for Galactic absorption, is $\sim 1.4 \times 10^{-11} \text{ erg cm}^{-2} \text{ s}^{-1}$. The luminosities in the 0.3–10 keV and 2–10 keV bands are $1.28 \times 10^{44} \text{ erg s}^{-1}$ and $0.43 \times 10^{44} \text{ erg s}^{-1}$, respectively. I Zw 1 is ~ 35 per cent dimmer than it was in 2002.

6 A REFLECTION INTERPRETATION FOR I Zw 1

6.1 The 2005 observation

The spectrum of I Zw 1 is power law dominated, but there is the necessity for a small contribution from a soft component below ~ 2 keV. The ionised disc reflection model (Ross & Fabian 2005) blurred by relativistic effects has had relatively good success in duplicating the appearance of the soft excess (e.g. Crummy et al. 2006).

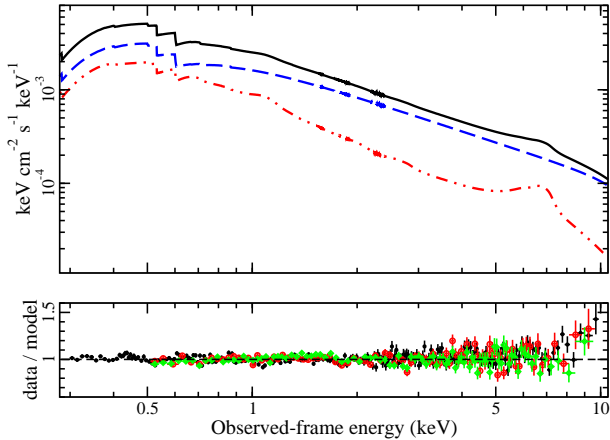


Figure 7. Top panel: The best fit blurred reflection model (only the pn model is shown for clarity). The reflection (red, dash-dot curve) and power law (blue, dashed curve) components, which make up the combined fit (black, solid curve) are presented. Bottom panel: The residuals of the model to the EPIC spectra. Symbols are as defined in Figure 6.

Table 2. The blurred reflection and power law model (with absorption) applied to the 2005 EPIC spectra ($\chi^2_{\nu}/\text{dof} = 1.10/1627$). The absorption parameters are as defined in Table 1. The blurring parameters are the emissivity index (α); inner (R_{in}) and outer (R_{out}) disc radius in gravitational radii ($r_g = GM/c^2$); and disc inclination (i). The iron abundance and ionisation parameter ($\xi = 4\pi F n^{-1}$, where F is the total incident flux and n is the hydrogen number density) of the reflector are also given.

(1) Model Component	(2) Fit Parameter
Absorption (neutral and ionised)	$N_{H_i} = 1.05^{+0.07}_{-0.13} \times 10^{20} \text{ cm}^{-2}$ $E = 638^{+7}_{-3} \text{ eV}$ $\tau = 0.30 \pm 0.01$
Power law	$\Gamma = 2.24 \pm 0.01$
Blurring	$\alpha = 2.48^{+0.36}_{-0.31}$ $R_{in} = 5.0^{+8.2}_{-1.6} r_g$ $R_{out} = 200 r_g$ (fixed) $i = 51 \pm 2^\circ$
Reflector	Fe = 1.1 ± 0.1 solar $\xi = 3060^{+107}_{-186} \text{ erg cm s}^{-1}$

As above, all the EPIC data were fitted with the blurred reflection plus power law model. Also, as in previous fits, we included an intrinsic neutral absorption component and an absorption edge as a pseudo-ionised absorber. As the model is complex, to simplify the fitting process the normalisations of the MOS spectra were linked to the pn spectrum and only a constant scale factor was used to correct for possible flux offsets between instruments. The incident spectrum for the reflection component was linked to that of the power law component.

The fit quality is not as satisfactory as some of the simple models ($\chi^2_{\nu}/\text{dof} = 1.10/1627$), but it does have the advantage of offering a physical explanation for the origin of the soft excess and

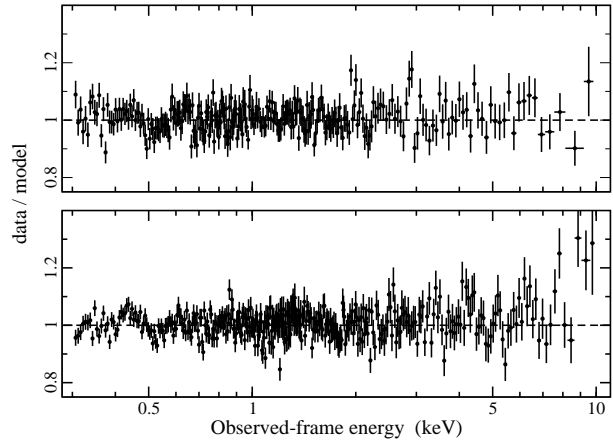


Figure 8. Residuals from a self-consistent power law plus blurred reflection model fitted simultaneously to the pn data from 2002 (top panel) and 2005 (bottom panel).

broad Fe K α line. Fit parameters are shown in Table 2, and the model along with fit residuals are presented in Figure 7. The fraction of reflected-to-total flux in the 0.3 – 10 keV range (corrected for Galactic and source absorption) is ~ 0.30 . Drawing conclusions from the fit parameters should probably be done with caution given the complexity of the low-energy absorption. However, it can be noted that the disc inner radius is not extremely small ($R_{in} = 5.0^{+8.2}_{-1.6} r_g$) and the emissivity profile is not very steep ($\alpha = 2.48^{+0.36}_{-0.31}$). Both points suggest that the reflection component does not necessarily originate from the innermost confines around the black hole as is suggested for many NLS1.

The advantage of this model is that it can account for the iron emission and soft excess in a self-consistent manner. Moreover, as will be discussed in Gallo et al. (2007), this reflection scenario can potentially explain some of the complicated spectral variability exhibited by I Zw 1.

6.2 Simultaneous fit to the 2002 and 2005 data

Based on the investigation in Section 4.2, most of the spectral differences between 2002 and 2005 can be associated with changes in the level of absorption. However, there do appear to be subtle changes in the shape of the continuum as well. As I Zw 1 was nearly twice as bright in 2002, in terms of the blurred reflection model the changes in the continuum shape could be interpreted as differing contributions from the direct power law component.

The data from both epochs were fitted simultaneously to examine consistency in the reflection scenario. For simplicity, many parameters were fixed to the best-fit 2005 values (see Table 3). The primary parameters that were left free for each dataset were the power law and absorption parameters, and the normalisation of the reflection component. The iron abundance and disc inclination were linked between the two spectra as large changes in these parameters would not be expected over 3-years. A reasonable fit can be achieved ($\chi^2_{\nu}/\text{dof} = 1.06/1480$) in this manner (see Figure 8 and Table 3).

As is seen in Table 3 there is no strong indication for a change in the shape of the direct power law component between 2002 and 2005. In addition, most of the blurring and reflection parameters

Table 3. The blurred reflection and power law model (with absorption) applied simultaneously to the 2002 and 2005 pn spectra ($\chi^2_{\nu}/\text{dof} = 1.06/1480$). The parameters are as defined in Table 2 and f marks the ones that are fixed in the fit. The 2002 and 2005 values are given in columns (2) and (3), respectively. The reflection (R) and flux fractions (F_R) (as defined in the text) are given in the final two rows.

(1) Model Component	(2) 2002	(3) 2005
Absorption (neutral and ionised)	$N_{\text{H}i} = 4.38^{+0.20}_{-0.19}$ $E = 623 \pm 10$ $\tau = 0.30^{+0.03}_{-0.04}$	$0.22^{+0.14}_{-0.17} \times 10^{20} \text{ cm}^{-2}$ $634^{+11}_{-6} \text{ eV}$ 0.23 ± 0.02
Power law	$\Gamma = 2.28 \pm 0.02$	$2.21^{+0.10}_{-0.08}$
Blurring	$\alpha = 2.48^f$ $R_{in} = 5.0^f$ $R_{out} = 200^f$ $i = 58 \pm 3^\circ$	2.48^f $5.0^f r_g$ $200^f r_g$ $58 \pm 3^\circ$
Reflector	$\text{Fe} = 1.10 \pm 0.13$ $\xi = 3060^f$	$1.10 \pm 0.13 \text{ solar}$ $3060^f \text{ erg cm s}^{-1}$
R	0.27 ± 0.04	0.45 ± 0.04
F_R	0.22 ± 0.03	0.31 ± 0.03

have been fixed. The most notable changes are in the amount of absorption (as noted in previous fits and by Costantini et al. 2007), the reflection fraction (R , fraction of reflected emission to power law emission in the 0.3–10 keV band), and in the level at which the reflection component contributes to the total 0.3–10 keV spectrum ($F_R = 0.22 \pm 0.03$ in 2002 and 0.31 ± 0.03 in 2005).

7 IRON LINE VARIABILITY

7.1 FeK α variability during the 2005 observation

The broad iron line in I Zw 1 has been detected in previous *ASCA* (Leighly 1999b) and *XMM-Newton* (G04) observations. In some respects, the clean detection of this clearly broad feature is another way that I Zw 1 differs from other NLS1.

In the analysis of G04 there were indications that the broad feature in the 2002 observation was composed of multiple (at least two) narrower emission lines. In the 2005 observation, the residuals can be fit by single Gaussian profile. Based on the width of the line ($\sigma = 523^{+276}_{-157} \text{ eV}$) in the EPIC spectra, the line-emitting region is between 12 – 66 r_g . Similar distance estimates come from the disc line fit and the blurred reflection model. Given the long observation and proximity of the line emitting region makes it plausible to search for line variability.

The mean pn spectrum was divided into 17 segments, each of 5 ks. The exposure in each segment was ~ 3.5 ks, taking account of the live-time of the pn camera in small window mode. The average number of source counts in the 5.5 – 7 keV band was slightly more than 200. The counts were grouped into spectra such that each bin contained at least 20 counts. For each 5 ks spectrum the continuum was determined by fitting the 4 – 10 keV band with a power law, while excluding the 5 – 7.2 keV range. The omitted band was replaced and the spectrum was rebinned into channels of 250 eV. Excess counts above the continuum in each 250 eV bin

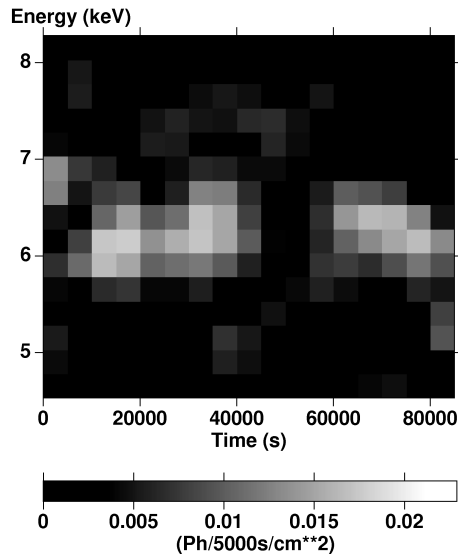


Figure 9. Excess-residual image for the 2005 pn spectrum in the 4.5 – 8.2 keV band. Bright spots indicate positive residuals in the spectrum, above a power law continuum. The time resolution is 5 ks, and the spectra are binned into 250 eV wide channels. The bright band between 5.8 – 6.7 keV corresponds to the broad emission line seen in the mean spectrum. The feature appears to be variable over the course of the observation.

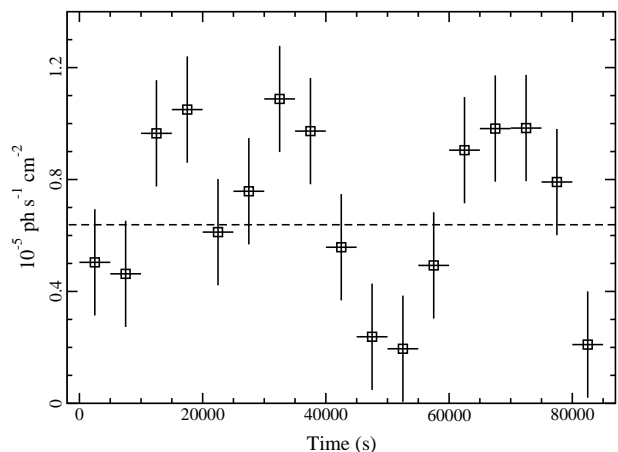


Figure 10. The light curve of the broad Fe K α emission in I Zw 1 during the 2005 observation. Bins are 5 ks. The 1- σ uncertainties were estimated as described in the text. A constant fit is shown for comparison.

were recorded. From this information an excess residual image was created as illustrated in Iwasawa et al. (2004; and in prep).

The resulting image from the 2005 observation is shown in Figure 9 and clearly indicates that the broad-line flux is variable. Most notably, the line flux diminishes significantly 45 – 60 ks from the start of the observation.

To create a light curve from the image, the excess counts between 5.8 – 6.7 keV were accumulated. Uncertainties on the light-curve data points were estimated from Monte Carlo simulations of the excess residual image. One-thousand images were created in an identical manner as done for I Zw 1. The spectra from which the images were derived were simulated for identical conditions as the

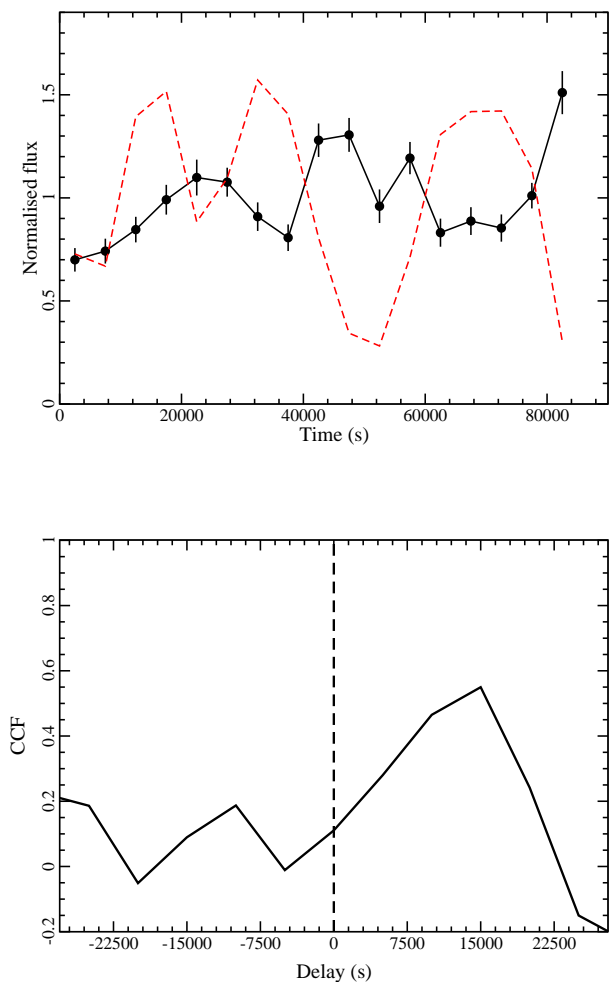


Figure 11. Top panel: The normalised light curve of the 6 – 10 keV continuum used to establish the iron line variations. The FeK α data shown in Figure 10 are normalised and overplotted (red, dashed curve). Bins are 5 ks. The 1- σ uncertainties on the continuum data points are taken from the 6 – 10 keV count rate. Lower panel: The CCF of the two light curves shown in the top panel. A positive delay indicates that the continuum changes lead the emission line variations.

2005 observation, assuming a power law plus stationary Gaussian profile. The uncertainty in the observed light curve was taken to be the standard deviation in the excess counts resulting from the simulated images. Details of the process including caveats are discussed in Iwasawa et al. (2004).

The Fe K α light curve shows clear variability (Figure 10) with a constant fit being unacceptable ($\chi^2_{\nu} = 2.45$). The fractional variability amplitude (F_{var} , using uncertainties derived in Edelson et al. 2002) is 34.8 ± 9.7 per cent.

A light curve of the 6 – 10 keV continuum was generated based on the power law fits used to derive the Fe K α light curve. The uncertainties in the 6 – 10 keV flux were assumed to be the same as the uncertainty in the corresponding count rate. The light curve, normalised to the average flux, is shown in Figure 11 with the broad-line light curve (Figure 10), also normalised, overplotted as a dashed curve. Interestingly, the curves appear to be anti-correlated in some parts of the light curve. Cross-correlating the broad-line and 6 – 10 keV continuum light curves indicates a weak

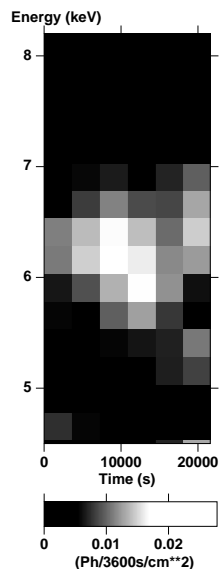


Figure 12. Excess-residual image for the 2002 pn spectrum in the 4.5 – 8.2 keV band. Bright spots indicate positive residuals in the spectrum, above a power law continuum. The time resolution is 3.6 ks, and the spectra are binned into 250 eV wide channels. The bright band between 6.0 – 6.5 keV corresponds to the broad emission line seen in the mean spectrum. Between 10 – 15 ks there is also brightening in the 5.5 – 6.0 keV band.

correlation with the broad-line light curve lagging the continuum fluctuations by ~ 15 ks (lower panel Figure 11).

The fractional variability in the 6 – 10 keV continuum is $F_{\text{var}} = 20.8 \pm 4.0$ per cent, less than the F_{var} in the Fe K α line. Statistically, the amplitude of the continuum variations is consistent with the Fe K α variations within about 2- σ . However, the difference is likely larger since the uncertainties on F_{var} are conservatively over-estimated (Edelson et al. 2002).

7.2 Revisiting the Fe K α variability in 2002

In fitting the spectra in various segments of the 2002 observation, G04 found little evidence of intensity variations in the broad-line. We take advantage of the excess-residual technique to re-examine the broad-line variability in the 2002 observation. An excess-residual image has been created for the 2002 pn observation in a nearly identical manner as was done for the 2005 observation. The only difference is that the time resolution is slightly better during 2002 because the mean spectrum was divided into 6 segments of 3.6 ks each (rather than 5 ks). This can be done without degrading the data quality because the 2002 observation was conducted in large-window mode, which has a CCD live-time of ~ 95 per cent; therefore the actual exposure in each segment of the 2002 observation is almost the same as the exposure in each segment of the 2005 data.

The 2002 excess-residual image is shown in Figure 12. The broad-line is dominant in the 6.0 – 6.5 keV range, but there is also apparent brightening that occurs in the 5.5 – 6.0 keV band between 10 – 15 ks. This is of particular interest because the continuum light curve shows a hard X-ray flare that peaks during this time interval (see G04).

Light curves were extracted from the excess-residual image in the 6.0 – 6.5 keV (blue line) and 5.5 – 6.0 keV (red line) bands. They were then normalised to their respective means and plot-

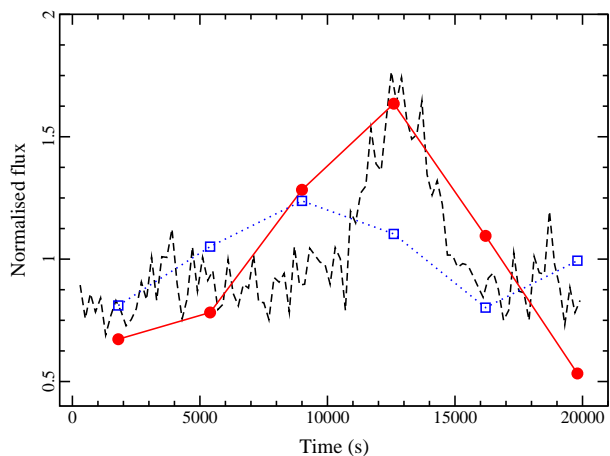


Figure 13. Various light curves from the 2002 observation of I Zw 1 normalised to their respective averages. The black, dashed curve is the 3 – 12 keV continuum light curve highlighting the hard X-ray flare reported previously by G04 (uncertainties in the curve are found in G04). The filled, red circles connected by a solid line mark the light curve extracted from the residual image (Figure 12) in the 5.5 – 6.0 keV range (i.e. the red line). The peak intensity in the red line corresponds with the peak intensity in the 3 – 12 keV continuum light curve. The open, blue squares connected by a dotted line is the light curve extracted from the residual image in the 6.0 – 6.5 keV band (i.e. the blue line).

ted with the normalised 2002 3 – 12 keV continuum light curve (Figure 13). As the observation was so short uncertainties in the residual-image light curves were not derived in a robust manner as was done for the 2005 data. We also note that propagation of Poisson uncertainties in each data bin yields very large error bars (on the order of 100 per cent), therefore we are only illustrating a trend in Figure 13.

The light curves suggest that the variations are more intense in the red line than in the blue line. There also is no obvious connection between the blue line light curve and that of the continuum. On the other hand, the red-line variations appear to be well correlated with the high-energy continuum variations and, despite the unknown size of the true error bars in the red line curve, the trend is obvious.

8 DISCUSSION

8.1 Time lags

The average CCFs calculated in Section 3 show a tendency for positive lags (hard band following soft band). This phenomenon has been observed in other AGN and Galactic black holes. However the origin of the lags is not certain.

In a simple corona with a uniform temperature and optical depth, variations can result from fluctuations in the intensity of the seed photons. Variations of this nature should produce fixed delays between low- and high-energy bands, resulting in a common time delay for all Fourier components. We do not estimate time lags as a function of frequency in I Zw 1; however the broad, asymmetric CCFs suggest that we do not have a single, well defined delay between the various energy bands. Examination of normalised light curves in different energy bands further supports this. A time lag

is only seen in parts of the light curves. In fact, at times the light curves are not correlated, or are actually anti-correlated.

Lags are seen in Cyg X-1, which can be attributed to spectral evolution in magnetic flares as they detach from the accretion disc (e.g. Poutanen & Fabian 1999). Another possibility is that the lags are manifested by material that propagates toward the black hole from regions of soft X-ray emission to regions of hard X-ray emission (e.g. Böttcher & Liang 1999; Kotov et al. 2001).

Based on the observation of another NLS1, IRAS 13224+3809, Gallo et al. (2004b) claimed a lag that alternated (sometimes hard band followed other times it led), with possible dependency on the average flux of the source. There is likely similar behaviour here as the first notable lag coincides with a sharp flux dip in the light curve about 25 ks into the observation.

8.2 Diminished neutral absorption since 2002

There is detectable diminishing of the intrinsic column density in I Zw 1 since 2002. The exact change depends on what continuum model is assumed, but appears to be at least on the 50 per cent level.

Changes in the neutral column density have been reported in several type 2 (i.e. absorbed) AGN (e.g. Risaliti et al. 2002), but to the best of our knowledge not in a NLS1. I Zw 1 is a merging and starburst system so there are several sources of absorption that exist in the galaxy and could feasibly change (e.g. due to bulk motion or dissipation of an absorbing component) over the span of a few years, which separates the two observations.

8.3 Origin of the Fe $K\alpha$ variability

8.3.1 Flux variations in the 2005 observation

The broad Fe $K\alpha$ line in I Zw 1 shows remarkable short-term variability. Understanding the origin of this variability is challenging.

Figure 11 suggests that the emission line and continuum variations could be correlated if we consider the iron-line fluctuations to lag the continuum by 10 – 12 ks. Such a delay would place the iron-line emitting region at approximately $180 r_g$ in I Zw 1. The distance is too large to account for the width of the iron feature which based on various spectral fits (e.g. Gaussian profile, disc line profile, blurred ionised reflector), originates within about $60 r_g$. A second problem is that the amplitude of the variations appears to be larger in the Fe $K\alpha$ line than in the 6 – 10 keV continuum that would be producing it. Even if we assume that the amplitudes of the variations are identical, it would be unlikely that all of the incident continuum will be reprocessed by the iron producing region and then emitted back into our line-of-sight.

Another possibility is that the variations are a result of some extrinsic effect rather than intrinsic changes in the line-emitting region. For example, motion within the accretion disc could account for some of the flux changes (e.g. Iwasawa et al. 2004). In this case, one would expect energy modulation in the excess residual map, which are not present in Figure 9. However, the strength of the modulations is dependent on the distance of the line-emitting region from the black hole and the disc inclination. It could be that in I Zw 1 this combination of parameters does not generate observable modulations.

In a speculative approach, we fit the Fe $K\alpha$ line light curve (Figure 10) with a sine curve. The fit was statistically good ($\chi^2_\nu = 1.02$) and the implied period was 49.1 ks. If the 49.1 ks corresponds to the orbital period of the emitting region around the black hole, then we can estimate the distance (e.g. following Bardeen et

al. 1972) to be $\sim 25 r_g$. This distance is consistent with that estimated from the width of the broad Fe $K\alpha$ line in the spectral models, but it is not clear why only the line-emitting region is affected in this manner and not the continuum.

Finally, the Fe $K\alpha$ variations could be due to variations in some optically-thick absorber in the line-emitting region. Such obscuring material could be created from instabilities in the accretion disc of highly inhomogeneous flows (e.g. Merloni et al. 2006).

8.3.2 Energy and flux variations in the 2002 observation

The most impressive feature in the 2002 continuum light curve of I Zw 1 was a modest X-ray flare concentrated in the 3 – 12 keV band. The blue line (6.0 – 6.5 keV) in I Zw 1 is not particularly variable and demonstrates no connection to the continuum variations. This behaviour is typical of other results (e.g. Iwasawa et al. 2004). However, the red line (5.5 – 6.0 keV) exhibits more intense variations which mimic the continuum light curve. In particular, the peak intensity in the red line corresponds well with the peak of the hard X-ray flare.

Due to limited data, examination of time-resolved spectra during 2002 do not yield significant results. The likely correlation between the continuum and red-line light curve suggests that the red line is Fe $K\alpha$ emission, which is produced in a spot on the accretion disc that is illuminated by the X-ray flare (i.e. perhaps co-rotating with the disc). The blue-line emission is representative of the average broad-line emission, which is produced at distances of $\sim 35 r_g$ as suggested by its width. The red-line emission and hard X-ray flare are generated closer to the black hole where Doppler and gravitational effects are more intense than the region where the blue line is produced (i.e. $< 35 r_g$).

It is worth noting that the red line could be related to the narrow 6.4 keV (6 keV observed-frame) emission feature that was identified in the 2002 spectrum by G04. Since the feature was not detected in the 2005 spectrum its origin could be connected to the transient red line (perhaps the blue-wing of this line), which is produced during the X-ray flare.

The combination of a hard X-ray flare, and redshifted and broadened Fe $K\alpha$ emission line has been seen in a very similar object, Nab 0205+024 (Gallo et al. 2004c). However, due to limited data, time-resolved spectral modelling did not yield information about possible line variability. Re-examination of the Nab 0205+024 data making use of excess residual imaging may be fruitful.

8.4 Physical models for I Zw 1

The level of absorption (neutral and ionised) appears to have changed between the two epochs. However, even after considering this there does seem to be some subtle change in the intrinsic continuum shape.

It is of interest to compare the changes in the context of a physical model such as reflection and light bending. In terms of the blurred reflection model, most of the intrinsic changes can be understood as arising from different relative contributions of the two continuum components. At both epochs (and historically), I Zw 1 appears to be in a power law dominated state – the soft excess is notably weak in this object.

If the power law component is a compact isotropic emitting source located above the black hole, as depicted in the light-bending scenario (e.g. Miniutti & Fabian 2004), then the changes

in the continuum shape are largely motivated by the proximity of this source to the black hole. In the higher flux 2002 observation, the contribution from the reflection component was less, and hence the soft excess was weaker. The AGN was brighter and in a power law dominated state. In 2005, I Zw 1 was dimmer and the reflection component (i.e. the soft excess) was stronger.

This is almost certainly a simplified description of the true situation. One would expect other spectral changes to occur as the power law component varies its distance from the black hole. For example, with increasing distance the photon index should harden (i.e. if due to Comptonisation), ionisation parameter may decrease as the accretion disc is less illuminated, and R_{in} will probably increase.

As the 0.3 – 10 keV spectrum of I Zw 1 is dominated by one component and subject to ionised absorption, it would not be surprising if other physical models provided adequate fits. Broad-band absorption models, like the blurred absorption models (e.g. Gierlinski & Done 2004), have not been examined in detail here, but could likely duplicate the spectrum of I Zw 1. It may be possible to break this degeneracy by examining the spectral variability, which is complex in I Zw 1 and is somewhat unlike what is seen in other NLS1 (Gallo et al. 2007).

9 CONCLUSIONS

In this work, we presented an 85 ks *XMM-Newton* observation and described the mean spectral and timing characteristics of the AGN, as well as compared the data to a previous, shorter *XMM-Newton* observation from 2002. The complex ionised absorber is discussed in detail in the work of Costantini et al. (2007). The remarkable spectral variability is presented in Gallo et al. (2007). The main findings from this work are the following.

(1) I Zw 1 is ~ 35 per cent dimmer in 2005 than it was in 2002. Between the two epochs the level of neutral column density intrinsic to I Zw 1 changed, as well as the ionised absorber. In addition, subtle changes in the continuum shape are apparent. If modelled with the blurred reflection model, the long-term continuum changes can be understood as arising from different relative contributions of the two continuum components (i.e. direct power law and ionised reflection).

(2) Variability is prevalent in all X-ray bands. The most distinct structure in the mean light curve is a flux dip ~ 25 ks into the observation. Average CCFs show a tendency for positive lags meaning soft band changes lead harder bands. However, examination of normalised light curves indicate that the high-energy variations are quite structured and lags are only apparent in some parts of the light curve. Interestingly, the hard X-ray lag first appears at the onset of the flux dip in the light curve. This possible alternating lag has been proposed for another NLS1 (IRAS 13224–3809, Gallo et al. 2004b) and it is not consistent with Comptonisation from a single corona with a uniform temperature and optical depth, and variable seed photons.

(3) The broad ionised Fe $K\alpha$ line shows significant variations over the course of the 2005 observation, which are not clearly due to intrinsic changes in the Fe $K\alpha$ -producing region. Other, viewer-perspective effects, such as orbital motion or absorption in the broad iron line-emitting region, could be invoked to describe the variability.

(4) The broad-line variability during 2002 is re-examined here. There is evidence suggesting that a relativistically broadened

Fe $K\alpha$ line is produced as a result of a hard X-ray flare illuminating the inner regions (i.e. $< 35 r_g$) of the accretion disc.

ACKNOWLEDGEMENTS

The *XMM-Newton* project is an ESA Science Mission with instruments and contributions directly funded by ESA Member States and the USA (NASA). The *XMM-Newton* project is supported by the Bundesministerium für Wirtschaft und Technologie/Deutsches Zentrum für Luft- und Raumfahrt (BMWi/DLR, FKZ 50 OX 0001), the Max-Planck Society and the Heidenhain-Stiftung. WNB acknowledges support from NASA LTSA grant NAG5-13035 and NASA grant NNG05GR05G.

REFERENCES

- Arnaud K., 1996, in: *Astronomical Data Analysis Software and Systems*, Jacoby G., Barnes J., eds, ASP Conf. Series Vol. 101, p17
- Arévalo P., Papadakis I. E., Uttley P., McHardy I. M., Brinkmann W., 2006, *MNRAS*, 372, 401
- Bardeen J. M., Press W. H., Teukolsky S. A., 1972, *ApJ*, 178, 347
- Böttcher M., Liang E. P., 1999, *ApJ*, 511, 37
- Crummy J., Fabian A., Gallo L., Ross R., 2006, *MNRAS*, 365, 1067
- den Herder J. W. et al. 2001, *A&A*, 365, 7
- Edelson R. A., Krolik J. H., 1988, *ApJ*, 333, 646
- Edelson R., Turner T. J., Pounds K., Vaughan S. Markowitz A., Marshall H., Dobbie P., Warwick R., 2002, *ApJ*, 568, 610
- Elvis M., Lockman F. J., Wilkes B. J., 1989, *AJ*, 97, 777
- Fabian A. C., Rees M. J., Stella L., White N. E., 1989, *MNRAS*, 238, 729
- Gallo L. C., Boller Th., Brandt W. N., Fabian A. C., Vaughan S., 2004a, *A&A*, 417, 29 (G04)
- Gallo L. C., Boller Th., Tanaka Y., Fabian A. C., Brandt W. N., Welsh W. F., Anabuki N., Haba Y., 2004b, *MNRAS*, 347, 269
- Gallo L. C., Boller Th., Brandt W. N., Fabian A. C., Vaughan S., 2004c, *MNRAS*, 355, 330
- Gierlinski M., Done C., 2004, *MNRAS*, 349, 7
- Iwasawa K., Miniutti G., Fabian A., 2004, *MNRAS*, 355, 1073
- Jansen F. et al. 2001, *A&A*, 365, L1
- Kotov O., Churazov E., Gilfanov M., 2001, *MNRAS*, 327, 799
- Leighly K., 1999a, *ApJS*, 125, 297
- Leighly K., 1999b, *ApJS*, 125, 317
- Mason K. O. et al. 2001, *A&A*, 365, 36
- Merloni A., Malzac J., Fabian A. C., Ross R. R., 2006, *MNRAS*, 370, 1699
- Miniutti G., Fabian A. C., 2004, *MNRAS*, 349, 1435
- Nowak M. A., Vaughan B. A., Wilms J., Dove J. B., Begelman, M. C. 1999, *ApJ*, 510, 874
- Papadakis I. E., Nandra K., Kazanas D., 2001, *ApJ*, 554, 133
- Poutanen J., Fabian, A. C., 1999, *MNRAS*, 306, 31
- Risaliti G., Elvis M., Nicastro F., 2002, *ApJ*, 571, 234
- Ross R. R., Fabian A. C., 2005, *MNRAS*, 358, 211
- Strüder L. et al. 2001, *A&A*, 365, L18
- Turner, M. J. L. et al. 2001, *A&A*, 365, 27

This paper has been typeset from a $\text{\TeX}/\text{\LaTeX}$ file prepared by the author.